IEEE Access
Multidisciplinary | Rapid Review | Open Access Journal

Received 14 June 2022, accepted 19 July 2022, date of publication 29 July 2022, date of current version 3 August 2022.

Digital Object Identifier 10.1109/ACCESS.2022.3195047

RESEARCH ARTICLE

Novel PM-Assisted Synchronous Reluctance Machines Using Asymmetrical Rotor Configuration

YING XIE, (Senior Member, IEEE), JIAWEI SHAO, SHOUCONG HE, BITIAN YE, FAN YANG, AND LIJING WANG

Electrical and Electronic Engineering Department, Harbin University of Science and Technology, Harbin 150080, China

Corresponding author: Ying Xie (xieying_1975@163.com)

This work was supported by the National Natural Science Foundation of China under Grant 51977052 and Grant U21A20145.

ABSTRACT This paper proposes a novel asymmetrical permanent magnet assisted synchronous reluctance machine (APMA-SynRM) with high cost performance, namely it has the advantages of high torque performance and low cost. This machine has an asymmetrical rotor configuration featured by low-cost ferrite and expensive NdFeB, and two kinds of material are placed asymmetrically on both sides of the ''U''-shaped barriers, which causes the magnet-axis-shift (MAS) effect. Consequently, the proposed APMA-SynRM improves the utilization of the reluctance torque and permanent magnet torque. The influences of permanent magnet volume ratio and hybrid permanent magnet on torque performance are further investigated, and the optimal topologies are designed through a multi-objective genetic algorithm. Moreover, the machine performance of APMA-SynRM is analyzed and compared with that of the conventional permanent magnet assisted synchronous reluctance machine (PMA-SynRM), which confirms that the proposed APMA-SynRM can reduce the cost of permanent magnets but still achieve similar torque and wider constant power speed range performance.

INDEX TERMS Asymmetrical rotor configuration, permanent magnet assisted synchronous reluctance machine (PMA-SynRM), magnet-axis-shift (MAS) effect, reluctance torque, permanent magnet torque.

I. INTRODUCTION

Recently, one of the current research hotspots for electric vehicles is permanent magnet synchronous machine (PMSM). As the cost of permanent magnets increases, the cost of PMSM increases accordingly [1]. In order to solve this problem, some scholars have reduced the dependence on rare earth magnets by increasing the ratio of reluctance torque. The synchronous reluctance machines do not use permanent magnets but their efficiency and power factor are low. Therefore, PMA-SynRM is proposed for combining the advantages of PMSM and the reluctance machine. With the wide speed range, high cost performance, and high efficiency of the PMA-SynRM gradually highlighted, electric vehicles, aerospace, household appliances and other fields began to pay attention to the development and application of the PMA-SynRM [2]–[4].

Compared with the machines without rare earth magnets, such as switched reluctance machines and synchronous reluctance machines, the torque performance of the PMA-SynRM which uses ferrite permanent magnet materials has greatly improved [5]. The rotor of PMA-SynRM usually adopts multi-layer flux barriers to obtain a high salient ratio and the position of the permanent magnets can affect torque performance [6]. Although ferrite permanent magnet materials are developing rapidly, there are still some weaknesses in performance compared with NdFeB. Thus, some researchers proposed to mix NdFeB with ferrite magnets to improve torque performance [7]. As a special PMSM, PMA-SynRM can produce relatively high reluctance torque and permanent magnet torque. But the utilization of two torque components is low because the current angles are different when they

The associate editor coordinating the review of this manuscript and approving it for publication was Kan Liu.

reach the maximum values. To solve the problem, various novel asymmetrical topologies with the magnet-axis-shift (MAS) effect are proposed [8]. Compared with conventional symmetrical PMSM, the PMSM with symmetrical permanent magnets and asymmetrical rotor core shows torque enhancement. It is demonstrated that an asymmetrical rotor core can achieve the MAS effect by shifting the position of the reluctance axis [9], [10]. Considering the torque performance improvement is not significant and mechanical stress issues, the geometry of asymmetrical permanent magnets and symmetrical rotor core is proposed [8]. The geometry is usually used in PMA-SynRM to maintain the merit of high reluctance torque while achieving the MAS effect [11], [12]. In order to take advantage of the MAS effect with more freedoms, the geometries of asymmetrical permanent magnets and asymmetrical rotor core are proposed in [13] and [14].

In this paper, the effect of the permanent magnet volume ratio on the torque performance is investigated to confirm that the MAS effect caused by the asymmetrical structure will improve the torque performance. On the basis of that, a novel APMA-SynRM is proposed, which has an asymmetrical rotor configuration featured by low-cost ferrite and expensive NdFeB, and two kinds of material are placed asymmetrically on both sides of the "U"-shaped barriers. Due to the MAS effect, this design can reduce the cost of permanent magnets by increasing the utilization of the reluctance torque and the permanent magnet torque. The main work of the article is organized as follows: section II shows the conventional PMA-SynRM topology and the proposed APMA-SynRM topology with an asymmetrical magnet arrangement. In section III, the 3-layer flux barrier is optimized through a global parametric optimization, then the effects of different permanent magnet volume ratios and hybrid permanent magnet on the torque performance are analyzed. In section IV, the machine performance of the proposed APMA-SynRM is compared and analyzed with that of the conventional PMA-SynRM. Finally, the conclusions are summarized in Section V.

II. MACHINE TOPOLOGY AND OPERATION PRINCIPLE

A. MACHINE TOPOLOGY

In Fig. 1, 48-slot/4-pole distributed winding is adopted in both the conventional PMA-SynRM and the proposed APMA-SynRM. Besides, they have the same rotor configuration with a 3-layer flux barrier per pole and stator configuration. In the conventional PMA-SynRM, all PMs inserted into the barriers are NdFeB magnets, whereas the proposed APMA-SynRM is designed by using two kinds of magnets, which are asymmetrically arranged.

B. MAGNET-AXIS-SHIFTING (MAS) EFFECT

To investigate the principle of MAS effect, a simplified analytic model is established by neglecting core saturation and cross-coupling. Fig. 2 shows the vector diagrams of PMA-SynRM and APMA-SynRM in d-q axis coordinates.

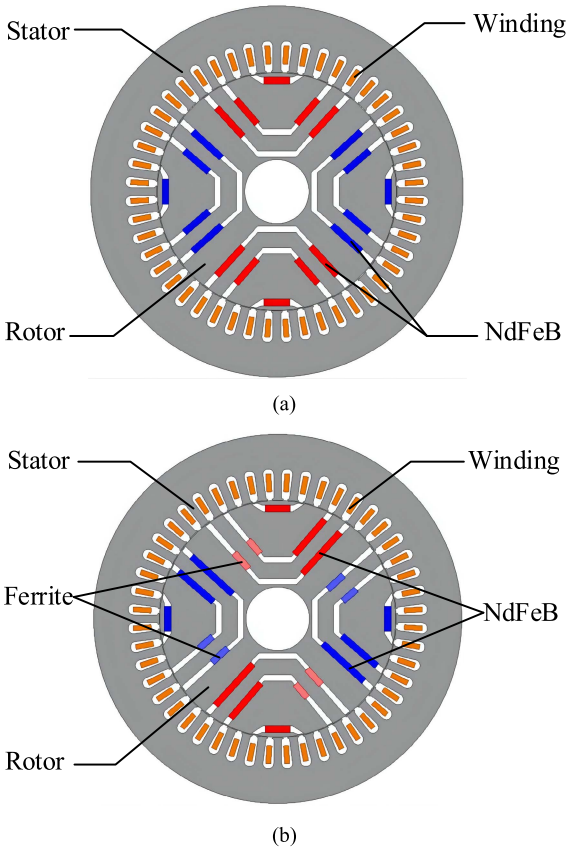

FIGURE 1. Machine topology. (a) Conventional PMA-SynRM (b) Proposed APMA-SynRM.

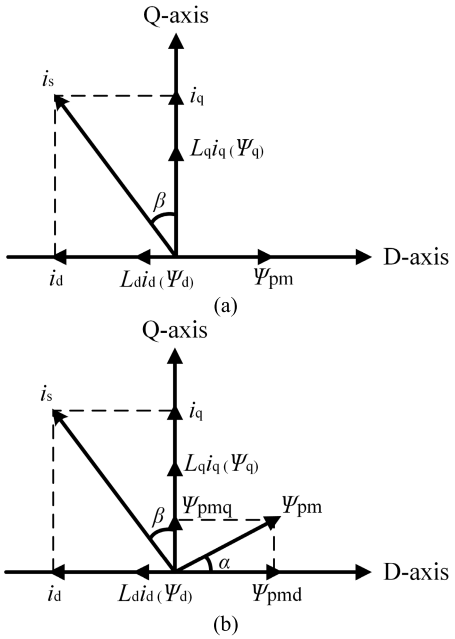

FIGURE 2. Vector diagrams. (a) Conventional PMA-SynRM (b) APMA-SynRM.

According to Fig. 2 (a), the permanent magnet flux linkages are opposite to the d-axis flux linkages generated by the stator current. Based on the constant coordinate

transformation of magnetic potential, the d- and q-axis flux linkages in PMA-SynRM are shown as (1),

$$\begin{cases} \psi_d = \psi_{pm} + L_d i_d \\ \psi_q = L_q i_q \end{cases} \tag{1}$$

where Ψ_d, Ψ_q and Ψ_{pm} are the d-axis flux linkage, q-axis flux linkage and permanent magnet flux linkage, L_d and L_q are the d-axis inductance and q-axis inductance, i_d and i_q are the d-axis current and q-axis current.

Furthermore, substitute stator current i_s and current advancing angle β into equation (1),

$$\begin{cases} \psi_d = \psi_{pm} - L_d i_s \sin\beta \\ \psi_q = L_q i_s \cos\beta \end{cases} \tag{2}$$

The torque equations of conventional PMA-SynRM are

$$\begin{cases} T_{yc} = \dfrac{3p}{2}\psi_{pm} i_q = \dfrac{3p}{2}\psi_{pm} i_s \cos\beta \\ T_{cz} = \dfrac{3p}{2}(L_q - L_d) i_d i_q = \dfrac{3p}{4}(L_q - L_d) i_s^2 \sin 2\beta \\ T_e = T_{yc} + T_{cz} \end{cases} \tag{3}$$

where T_{yc}, T_{cz}, T_e are the PM, reluctance and synthetic torque components, p is the number of pole pairs.

According to Fig. 2 (b), as the permanent magnets in the proposed APMA-SynRM are no longer arranged symmetrically, the permanent magnet flux linkages are shifted by a certain angle compared with Fig. 2 (a), which is defined as α. Based on the constant coordinate transformation of magnetic potential, the d-axis flux linkage and q-axis flux linkage in APMA-SynRM are expressed as (4) and (5).

$$\begin{cases} \psi_d = L_d i_d + \psi_{pmd} \\ \psi_q = L_q i_q + \psi_{pmq} \end{cases} \tag{4}$$

$$\begin{cases} \psi_d = \psi_{pm}\cos\alpha - L_d i_s \sin\beta \\ \psi_q = \psi_{pm}\sin\alpha + L_q i_s \cos\beta \end{cases} \tag{5}$$

The torque equations of APMA-SynRM are

$$\begin{cases} T_{yc} = \dfrac{3p}{2}\psi_{pmd} i_q - \dfrac{3p}{2}\psi_{pmq} i_d = \dfrac{3p}{2}\psi_{pm} i_s \cos(\beta - \alpha) \\ T_{cz} = \dfrac{3p}{2}(L_q - L_d) i_d i_q = \dfrac{3p}{4}(L_q - L_d) i_s^2 \sin 2\beta \\ T_e = T_{yc} + T_{cz} \end{cases} \tag{6}$$

where Ψ_{pmd} and Ψ_{pmq} are the d- and q-axis permanent magnet flux linkage.

According to formulas (3) and (6), the torque characteristics of PMA-SynRM and APMA-SynRM are compared in Fig. 3. Both the torque components are not fully utilized (see in Fig. 3 (a)) because the difference in current angles is 45 electrical degrees (ED) when the PM torque and reluctance torque reach the maximum values. Due to the MAS effect caused by asymmetrical structure, the PM torque will be shifted. The direction of the MAS is determined by the asymmetrical structure. In order to improve the torque performance, it is hoped that the MAS will make PM torque and reluctance torque reach the maximum values at a similar current angle, as shown in Fig. 3 (b). Thus, the synthetic torque is enhanced by increasing the utilization of the two torque components.

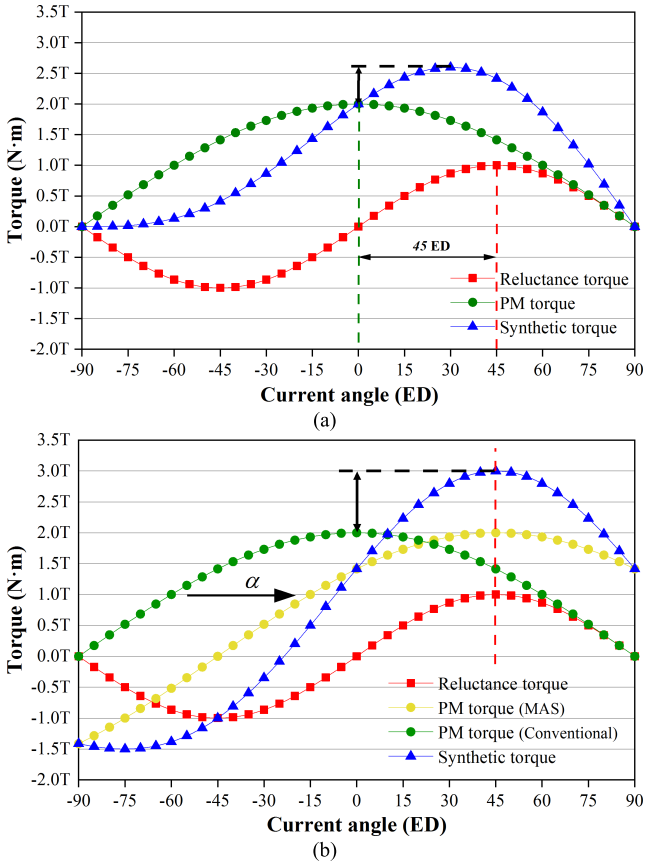

FIGURE 3. Torque characteristics. (a) PMA-SynRM (b) APMA-SynRM.

C. TORQUE SEGREGATION USING FPM

To further analyze the influence of the MAS on torque performance, reluctance torque and PM torque should be separated from total torque. In general, maxwell stress tensor and virtual work principle are used for torque calculation [15]. However, taking magnetic saturation and cross-coupling into consideration, the total flux linkage cannot be linearly decomposed [16]. So FPM is adopted to separate electromagnetic torque. Fig. 4 shows the steps of torque separation using FPM. Firstly, the electromagnetic torque will be obtained with all excitation (PM and current). Then, permanent magnets are substituted with air to obtain reluctance torque. Finally, the PM torque is obtained by subtracting reluctance torque from the electromagnetic torque.

III. DESIGN OPTIMIZATION

A. GLOBAL PARAMETRIC OPTIMIZATION

The conventional PMA-SynRM and the proposed APMA-SynRM are designed based on the condition that the stator and multi-layer flux barrier structures are identical. Therefore, the multi-layer flux barrier is optimized through a

multi-objective optimization to obtain the optimal topology of PMA-SynRM and prepare for the proposed APMA-SynRM. The design variables of multi-layer flux barrier structures are shown in Fig. 5.

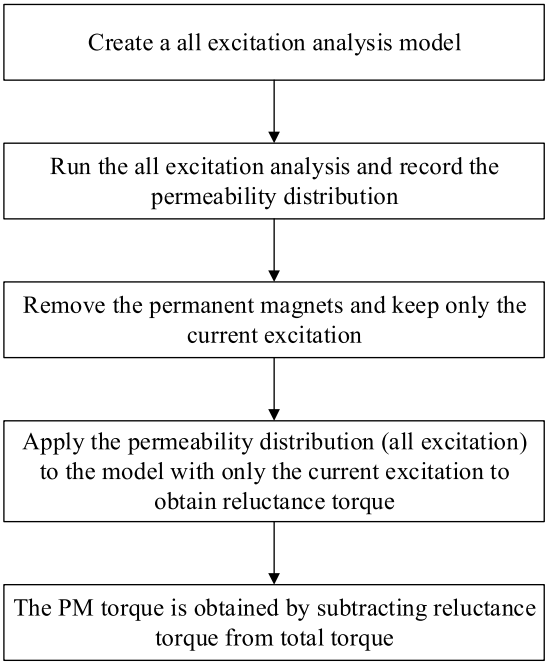

FIGURE 4. The steps of torque separation using FPM.

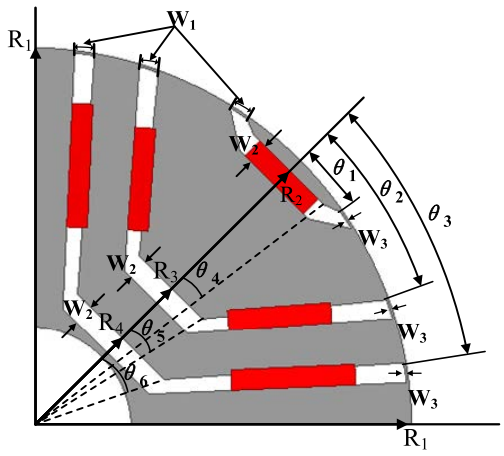

FIGURE 5. The design variables of the conventional PMA-SynRM.

According to Fig. 5, R_1 is the outer diameter of rotor, R_2, R_3, R_4 are the diameter of the flux barriers, $\theta_1, \theta_2, \theta_3$ are the opening angle of the flux barriers, $\theta_4, \theta_5, \theta_6$ are the width of the flux barrier bottom, W_1 represents the thickness of the flux barrier arm, W_2 represents the thickness of the flux barrier bottom, W_3 represents the bridge thickness of the flux barrier. Based on a comprehensive consideration of the higher average torque and lower torque ripple, the optimal design parameters are selected in Fig. 6. Table 1 shows the data of the final optimal design.

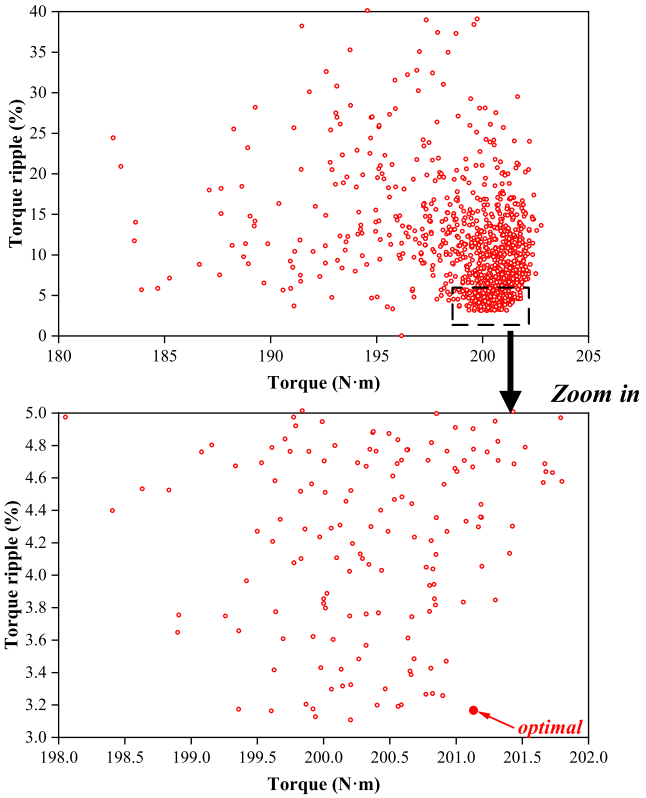

FIGURE 6. Global optimization results of the conventional PMA-SynRM.

TABLE 1. Design variables.

Parameters	Unit	Optimal
R_1	mm	92.9
R_2	mm	89.6
R_3	mm	51.3
R_4	mm	35.7
θ_1	deg	10
θ_2	deg	25.4
θ_3	deg	34.8
θ_4	deg	7.5
θ_5	deg	12.5
θ_6	deg	25
W_1	deg	3
W_2	mm	5
W_3	mm	0.6

B. INFLUENCE OF PERMANENT MAGNET VOLUME RATIO ON TORQUE PERFORMANCE

After obtaining the optimal parameters, three machines are proposed on the basis of the conventional PMA-SynRM to verify the effect of different volume ratios on torque performance, as shown in Fig. 7.

Compared with the conventional PMA-SynRM, the three machines change the permanent magnet volume ratio on both sides of the magnetic barriers. The total volume of the permanent magnets remains the same and all PMs inserted into the barriers are NdFeB.

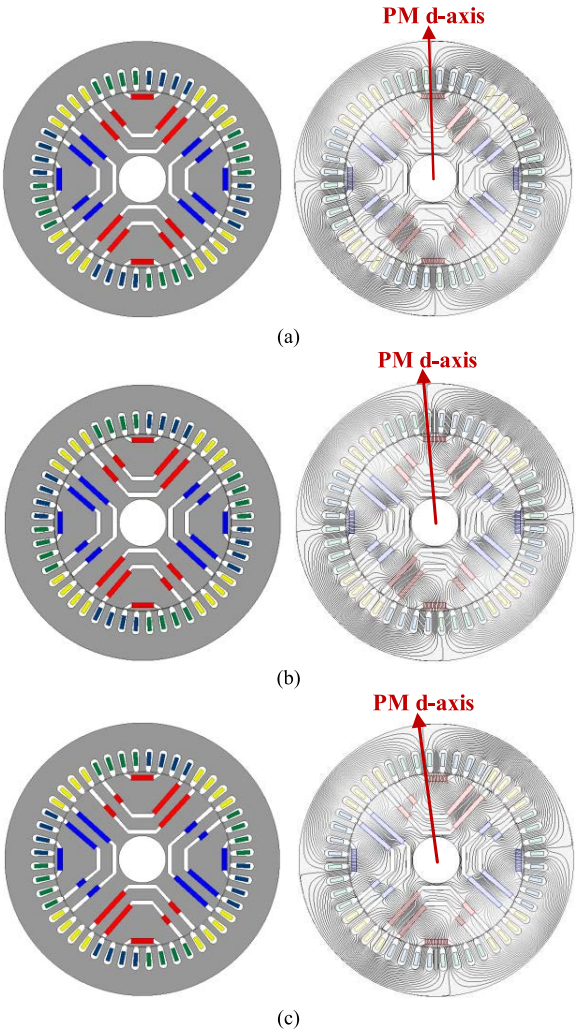

FIGURE 7. Machine Topology and open-circuit flux line distributions. (a) Machine I (b) Machine II (c) Machine III.

As the permanent magnets inside the flux barriers have the same thickness and axial length, the volume ratio γ can be defined as

$$\gamma = \frac{L_1 + L_2}{L_3 + L_4} \tag{7}$$

where L_1, L_2, L_3, and L_4 are the length of the permanent magnets, as described in Fig. 8.

As can be observed from the comparison of the open-circuit flux line distributions of the three machines, the angle of MAS will change when the volume ratio changes. In other words, when the degree of asymmetry increases, the angle of MAS also increases. Table 2 shows the average torque comparison of the three machines, which confirms that the torque performance will be changed by changing the volume ratio of the permanent magnets.

TABLE 2. Comparison of average torque with different volume ratios.

Item	Machine I	Machine II	Machine III
γ	9/13	7/15	5/17
Average torque	210.058 N·m	212.665 N·m	214.285 N·m

C. INFLUENCE OF HYBRID PERMANENT MAGNET ON TORQUE PERFORMANCE

To further research the effect of asymmetrical magnet arrangement on torque performance, the proposed APMA-SynRM is designed as a hybrid permanent magnet on the basis of changing the volume ratio (studied in section B), i.e., ferrite and NdFeB are placed asymmetrically on both sides of the "U"-shaped barriers. It aims to further increase the degree of asymmetry, which can compensate for the lack of ferrite performance through the MAS effect. The design parameters are shown in Fig. 8. L_5, L_6, L_7, and L_8 are the length between the center of the permanent magnets and the bottom of the flux barriers. The volume ratio and the position of the two materials are carried out by a multi-objective optimization, and the optimal parameters are selected in Fig. 9 by taking higher average torque and lower torque ripple into consideration. The design variables of the final optimal design and the conventional PMA-SynRM benchmark are shown in Table 3.

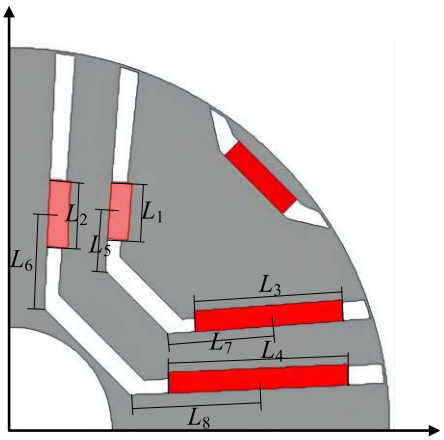

FIGURE 8. The design variables of the proposed APMA-SynRM.

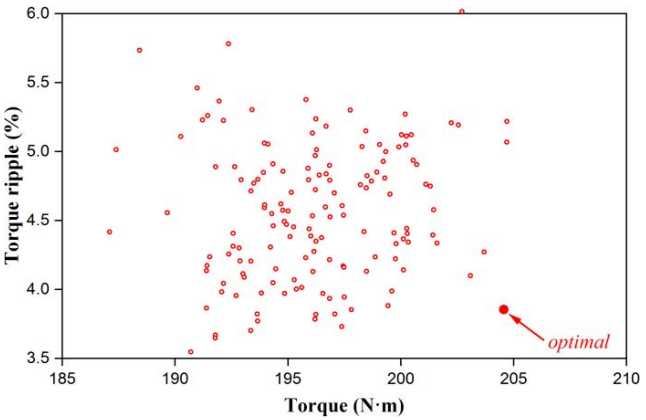

FIGURE 9. Multi-objective optimization results of the proposed APMA-SynRM.

IV. COMPARISON OF MACHINE PERFORMANCE

In order to confirm the feasibility of the proposed APMA-SynRM, the machine performances of the proposed APMA-SynRM and conventional PMA-SynRM, such as

TABLE 3. Design variables.

Parameters	Unit	Conventional	Proposed
L_1	mm	25	13.89
L_2	mm	30	16.27
L_3	mm	25	36.11
L_4	mm	30	43.73
L_5	mm	10	7.78
L_6	mm	20	15.16
L_7	mm	10	6.87
L_8	mm	20	9.74
γ	-	1	0.378

open-circuit performances, on-load torque performances and constant power speed range performances, are compared and analyzed in this section. Table 4 shows the major design data of the two machines.

TABLE 4. The major design data.

Item	Unit	Conventional	Proposed
Stator outer diameter	mm	240	240
Stator inner diameter	mm	187	187
Number of poles	-	4	4
Number of stator slots	-	48	48
Turns	-	30	30
Wire diameter	mm	1.3	1.3
Number of strands	-	2	2
Parallel number	-	2	2
Rated speed	r/min	1500	1500
Rated current	A	30	30
Air-gap length	mm	0.6	0.6
Lamination axial length	mm	240	240
Magnet material	-	NdFeB	NdFeB/ferrite
Steel sheet	-	DW310-35	DW310-35

A. OPEN-CIRCUIT PERFORMANCE

Fig. 10 compares the open-circuit flux line distributions of the PMA-SynRM and the APMA-SynRM. Fig. 11 compares the waveform and harmonic decomposition of the open-circuit air-gap flux density.

According to Fig. 10 and Fig. 11, it demonstrates that the PM d-axis is obviously shifted by the asymmetrical structure of the rotor, the angle of MAS is defined as α mechanical degree (MD). As can be observed from Fig. 11, the proposed APMA-SynRM shows a similar amplitude of open-circuit flux density waveform but significant distortions can be observed, the harmonic decomposition of the APMA-SynRM exhibits smaller fundamental components and larger higher-order harmonics, which are mainly due to the asymmetrical rotor structure.

Fig. 12 shows the waveform and harmonic decomposition of open-circuit back electro-motive force (EMF). The proposed APMA-SynRM shows significant distortion in the waveform and exhibits smaller fundamental components and

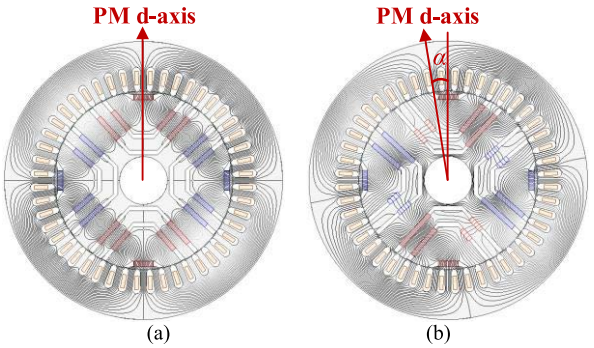

FIGURE 10. Open-circuit flux line distributions. (a) Conventional PMA-SynRM (b) Proposed APMA-SynRM.

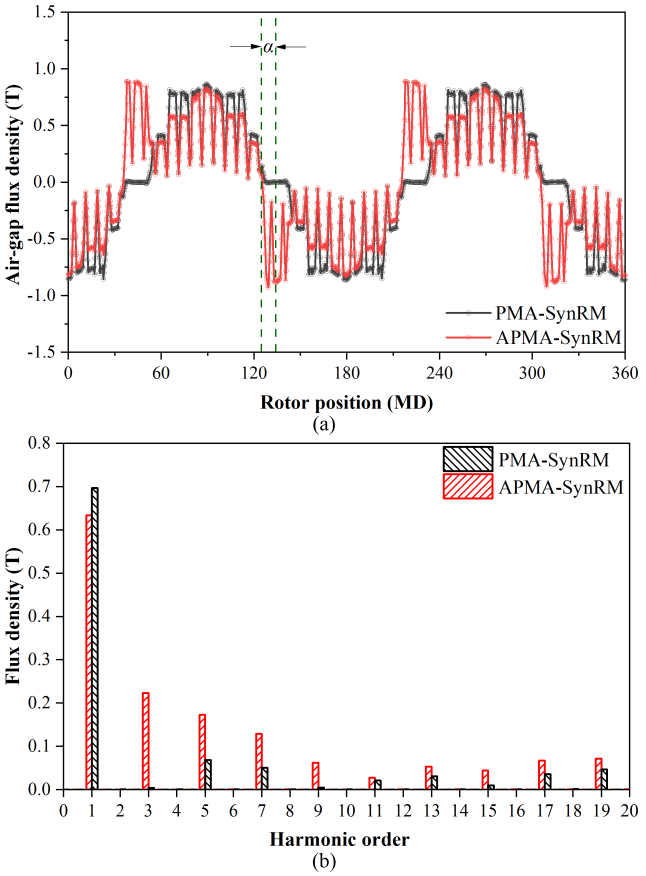

FIGURE 11. Open-circuit flux density comparisons in air-gap (a) Waveforms, (b) Harmonic decomposition.

larger higher-order harmonics in the spectra. In addition, its waveform is shifted by $p\alpha$ (ED), where p is the number of pole pairs.

B. ON-LOAD TORQUE PERFORMANCE

The torque performance of two machines at 30A and 1500 r/min is compared in Fig. 13. The proposed APMA-SynRM has a similar average torque but a slightly larger torque ripple than conventional PMA-SynRM. To research the influence of the MAS effect caused by

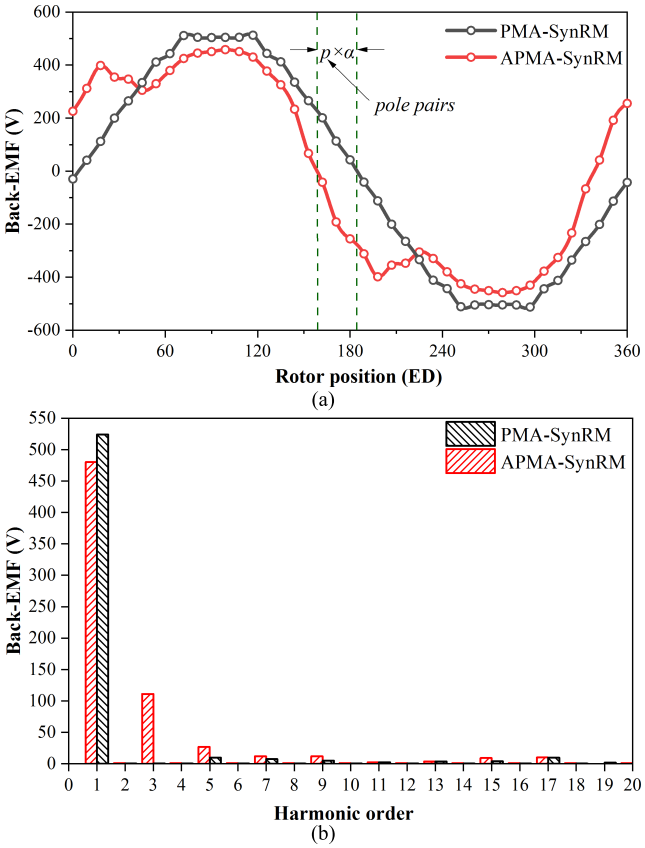

FIGURE 12. Open-circuit back-EMFs comparison. (a) Waveforms (b) Harmonic decomposition.

TABLE 5. Torque performance comparison of two machines.

Item	Unit	Conventional	Proposed
The volume of NdFeB	m^3	6.24×10^{-4}	4.7926×10^{-4}
The volume of ferrite	m^3	0	1.4474×10^{-4}
The total volume of PM	m^3	6.24×10^{-4}	6.24×10^{-4}
Maximum total torque	N·m	200.64	204.93
T_{pm}	N·m	61.38	65.64
$T_{pm\text{-}max}$	N·m	100.23	76.74
λ_{pm}	%	61.24	85.54
T_r	N·m	139.26	139.29
T_{r-max}	N·m	141.41	139.29
λ_r	%	98.48	100
The cost of PMs	¥	3001.44	2337.14

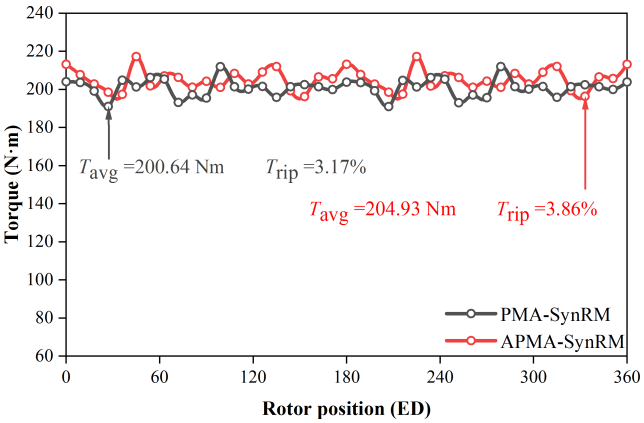

FIGURE 13. Torque waveforms with 30A current amplitude and 1500 r/min.

asymmetric rotor configuration on torque performance, the torque characteristics of both two machines are compared in Fig. 14, and the utilization of the reluctance torque and PM torque can be defined as

$$\begin{cases} \lambda_{pm} = \dfrac{T_{pm}}{T_{pm-max}} \times 100\% \\ \lambda_r = \dfrac{T_r}{T_{r-max}} \times 100\% \end{cases} \tag{8}$$

where λ_{pm} and λ_r are the utilization of the PM torque and reluctance torque, T_{pm} and T_r are the PM torque and reluctance torque when the synthetic torque reaches the maximum values. T_{pm-max} and T_{r-max} are the maximum values of the PM torque and reluctance torque. Table 5 compares the torque performance of the two machines. The two topologies have the similar T_{r-max} because of having the same 3-layer flux barriers. The proposed APMA-SynRM has a lower T_{pm-max} because of the low-performance ferrite. However, the proposed APMA-SynRM has higher utilization of the reluctance torque and PM torque compared with conventional PMA-SynRM. Consequently, the proposed APMA-SynRM can reduce the cost of permanent magnets by 22.13% while it can still obtain a similar torque.

As can be seen from the average torques versus input current amplitude in Fig. 15, the proposed APMA-SynRM has a similar average torque compared with the PMA-SynRM under the different applied loads.

C. CONSTANT POWER SPEED RANGE PERFORMANCE

For PMSM, a wide constant power speed range performance (CPSR) is as important as high torque/power density and high efficiency. To analyze the CPSR performance of the machines, the torque- and power-speed curves of the two machines are compared in Fig. 16 and the comparison of the efficiency map is shown in Fig. 17. In the calculation, the maximum current amplitude is limited to 45A (peak current) and both machines are controlled by maximum torque per ampere (MTPA).

As shown in Fig. 16, the proposed APMA-SynRM has a similar torque in the constant-torque region and it can also achieve a high speed. And the maximum power of the APMA-SynRM remains constant basically when the speed exceeds 2000 rpm. However, the maximum power of the PMA-SynRM starts to decrease after 2000 rpm. In Fig. 17, the efficiency of the proposed APMA-SynRM is slightly lower than the conventional PMA-SynRM. In conclusion, the proposed APMA-SynRM shows better CPSR performances than PMA-SynRM.

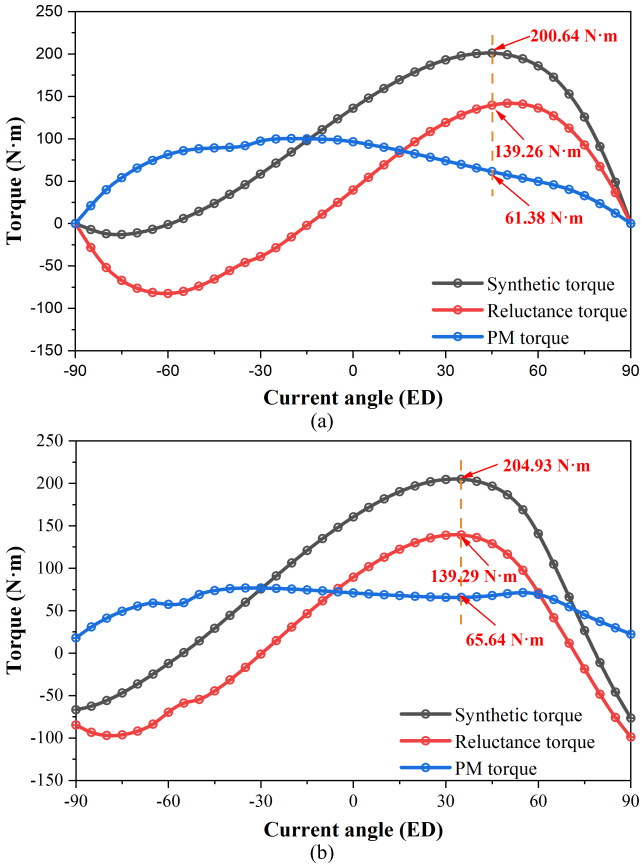

FIGURE 14. Torque characteristics. (a) Conventional PMA-SynRM (b) Proposed APMA-SynRM.

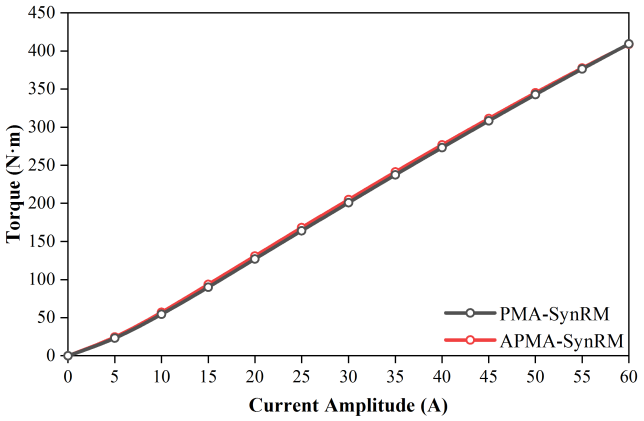

FIGURE 15. Maximum average torques versus current amplitude.

D. PERMANENT MAGNET DEMAGNETIZATION

In general, the small dimension permanent magnets are easier to lead to demagnetization. In addition, the proposed APMA-SynRM also uses ferrite which is easy to demagnetize. Thus, it is necessary to investigate the demagnetization of permanent magnets. When the armature excitation is set as 30A, the magnetic flux density of the magnets at 100°C is shown in Fig. 18. In order to research the demagnetization

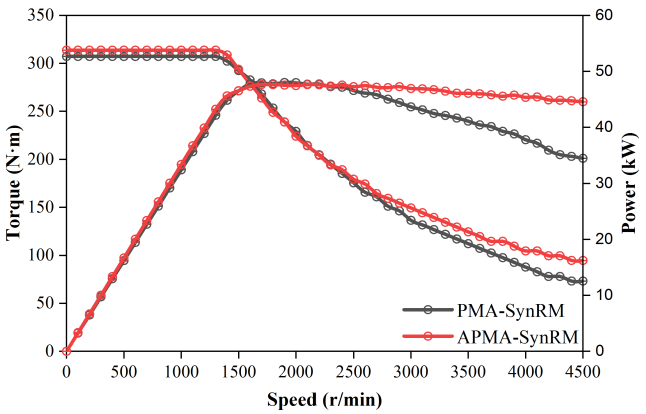

FIGURE 16. Torque and power-speed curves.

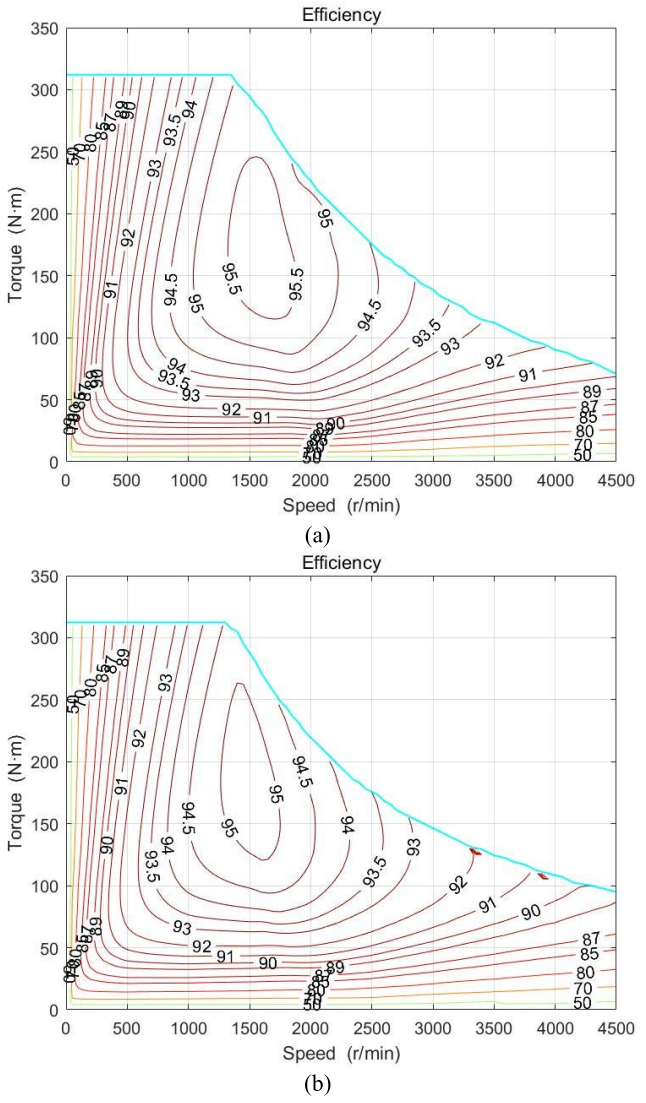

FIGURE 17. Efficiency maps. (a) Conventional PMA-SynRM (b) Proposed APMA-SynRM.

of the permanent magnets, five typical points that are easy to demagnetize are marked on the five permanent magnets.

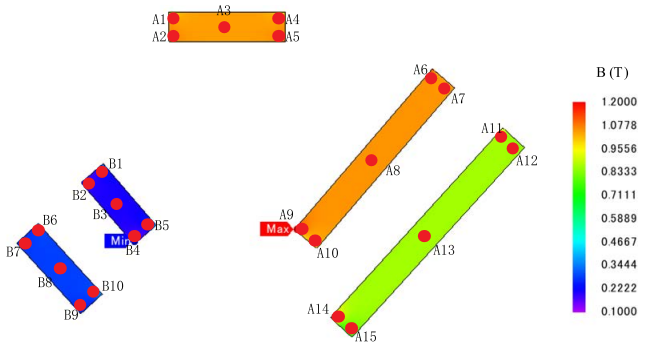

FIGURE 18. The magnetic flux density of the magnets at 100°C and 30A.

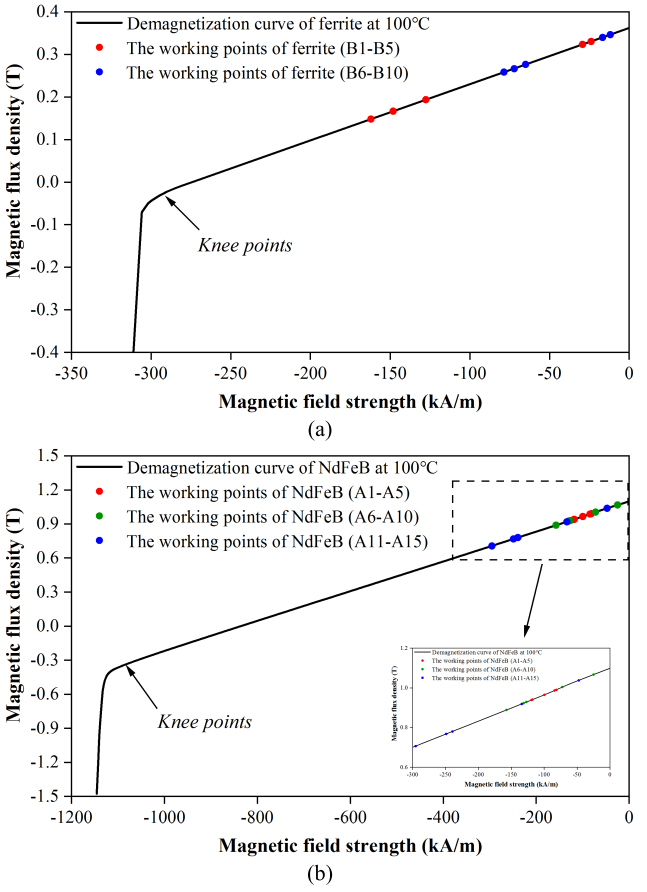

FIGURE 19. The working points of the ferrite and NdFeB magnets. (a) Ferrite (b) NdFeB.

When the temperatures of ferrite and NdFeB are adjusted as 100°C, their knee points are −0.02T and −0.32T, respectively. It is apparent that all the magnetic flux density of woking points are larger than the knee points, which reveals that the permanent magnets are immune to demagnetization under the normal operating condition. The magnetic flux density is simulated for each point, as shown in Fig. 19.

V. CONCLUSION

In this paper, a novel APMA-SynRM topology has been proposed. It has an asymmetrical rotor configuration to achieve the MAS effect. The machine performances of the proposed APMA-SynRM and the conventional PMA-SynRM are comprehensively compared and investigated by finite element analysis. As the two topologies have the same multi-layer flux barriers, they have the approximate $T_{\mathrm{r-max}}$. Due to the hybrid permanent magnet, the proposed APMA-SynRM reduces the usage of NdFeB and obtains a lower $T_{\mathrm{pm-max}}$. However, the proposed APMA-SynRM improves the utilization of the reluctance torque and PM torque to compensate for the lack of ferrite performance through the MAS effect. So, it can reduce the cost of permanent magnets by 22.13% while it can still achieve the similar torque compared with the conventional PMA-SynRM. In addition, due to the asymmetrical rotor structure, the proposed APMA-SynRM shows distortion and larger high-order harmonics in the waveforms and harmonic decomposition of the open-circuit air-gap flux density and back-EMF. Finally, the proposed APMA-SynRM has better CPSR performances, and the permanent magnets are immune to demagnetization under the normal operating condition.

REFERENCES

[1] N. Bianchi, E. Fornasiero, M. Ferrari, and M. Castiello, "Experimental comparison of PM-assisted synchronous reluctance motors," *IEEE Trans. Ind. Appl.*, vol. 52, no. 1, pp. 163–171, Jan./Feb. 2016.

[2] E. Trancho, E. Ibarra, A. Arias, I. Kortabarria, J. Jurgens, L. Marengo, A. Fricassé, and J. V. Gragger, "PM-assisted synchronous reluctance machine flux weakening control for EV and HEV applications," *IEEE Trans. Ind. Electron.*, vol. 65, no. 4, pp. 2986–2995, Apr. 2018.

[3] P. Li, W. Ding, and G. Liu, "Sensitivity analysis and design of a high performance permanent-magnet-assisted synchronous reluctance motor for EV application," in *Proc. IEEE Transp. Electrific. Conf. Exp. (ITEC)*, Long Beach, CA, USA, Jun. 2018, pp. 406–411.

[4] O. Payza, Y. Demir, and M. Aydin, "Investigation of losses for a concentrated winding high-speed permanent magnet-assisted synchronous reluctance motor for washing machine application," *IEEE Trans. Magn.*, vol. 54, no. 11, pp. 1–5, Nov. 2018.

[5] L. Knebl, J. Barta, J. Kurfurst, and C. Ondrusek, "High-torque ferrite synchronous reluctance machine design optimization," in *Proc. 19th Int. Conf. Mechtron. Mechatronika (ME)*, Dec. 2020, pp. 1–5.

[6] T. Mohanarajah, M. Nagrial, J. Rizk, and A. Hellany, "Permanent magnet optimization in PM assisted synchronous reluctance machines," in *Proc. IEEE 27th Int. Symp. Ind. Electron. (ISIE)*, Cairns, QLD, Australia, Jun. 2018, pp. 1347–1351.

[7] Z. S. Du and T. A. Lipo, "Cost-effective high torque density Bi-magnet machines utilizing rare Earth and ferrite permanent magnets," *IEEE Trans. Energy Convers.*, vol. 35, no. 3, pp. 1577–1584, Sep. 2020.

[8] Z.-Q. Zhu and Y. Xiao, "Novel magnetic-field-shifting techniques in asymmetric rotor pole interior PM machines with enhanced torque density," *IEEE Trans. Magn.*, vol. 58, no. 2, pp. 1–10, Feb. 2022.

[9] G. Liu, G. Xu, W. Zhao, X. Du, and Q. Chen, "Improvement of torque capability of permanent-magnet motor by using hybrid rotor configuration," *IEEE Trans. Energy Convers.*, vol. 32, no. 3, pp. 953–962, Sep. 2017.

[10] H. Yang, W. Wang, H. Lin, Z. Q. Zhu, S. Lyu, and S. Niu, "A novel hybrid-pole interior PM machine with magnet-axis-shifting effect," in *Proc. IEEE Int. Electric Mach. Drives Conf. (IEMDC)*, May 2019, pp. 273–279.

[11] S. Hayslett and E. Strangas, "Design and analysis of aligned axis interior permanent magnet machines considering saturation," in *Proc. IEEE Int. Electric Mach. Drives Conf. (IEMDC)*, May 2019, pp. 686–692.

[12] Y. Xiao, Z. Q. Zhu, J. T. Chen, D. Wu, and L. M. Gong, "A novel V-shape interior permanent magnet synchronous machine with asymmetric spoke-type flux barrier," in *Proc. Int. Conf. Electr. Mach. (ICEM)*, Aug. 2020, pp. 382–388.

[13] Y. Xiao, Z.-Q. Zhu, J.-T. Chen, D. Wu, and L.-M. Gong, "A novel asymmetric rotor interior PM machine with hybrid-layer PMs," in *Proc. IEEE Energy Convers. Congr. Exp. (ECCE)*, Oct. 2020, pp. 4029–4035.

[14] P. Winzer and M. Doppelbauer, "Comparison of synchronous machine designs with displaced reluctance axis considering losses and iron saturation," in *Proc. IEEE Int. Electric Mach. Drives Conf. (IEMDC)*, Coeur d'Alene, ID, USA, May 2015, pp. 1801–1807.
[15] Z. Q. Zhu and W. Q. Chu, "Advanced frozen permeability technique and applications in developing high performance electrical machines," *Trans. China Electrotech. Soc.*, vol. 31, no. 20, pp. 13–29, Oct. 2016.
[16] W. Q. Chu and Z. Q. Zhu, "Average torque separation in permanent magnet synchronous machines using frozen permeability," *IEEE Trans. Magn.*, vol. 49, no. 3, pp. 1202–1210, Oct. 2013.

YING XIE (Senior Member, IEEE) received the Ph.D. degree in electric machine and apparatus from the Harbin Institute of Technology, Harbin, China, in 2008.

She was a Postdoctoral Researcher at the Huazhong University of Science and Technology, Wuhan, China, from 2010 to 2012, and a Visiting Scholar at Sheffield University, U.K., in 2013. She is currently a Professor with the Harbin University of Science and Technology. Her current research interests include comprehensive physical fields calculation, including vibration characteristic and noise applied to electric motors, state monitoring and fault diagnosis of induction motors, and permanent magnet compound motors, and drives for new energy electric vehicles.

JIAWEI SHAO received the B.E. degree in electrical engineering and automation from the Harbin University of Science and Technology, Harbin, China, in 2020, where he is currently pursuing the M.E. degree in electric machine and apparatus. His current research interests include permanent magnet vernier synchronous motors design and permanent magnet assisted synchronous reluctance motors design.

SHOUCONG HE received the B.E. degree in electrical engineering and automation from the Jiangsu University of Science and Technology, Zhenjiang, China, in 2020. He is currently pursuing the M.E. degree in electric machine and apparatus with the Harbin University of Science and Technology, Harbin, China.

His current research interest includes permanent magnet vernier motors design and analysis.

BITIAN YE received the B.E. degree in electrical engineering and automation from Henan Polytechnic University, Jiaozuo, China, in 2019. He is currently pursuing the Ph.D. degree in electric machine and apparatus with the Harbin University of Science and Technology, Harbin, China. His current research interests include variable flux memory motors design and high-power and high-speed permanent magnet motors design.

FAN YANG received the B.E. degree in electrical engineering and automation from Linyi University, Linyi, China, in 2016, and the M.E. degree in electrical engineering from Northeast Petroleum University, Daqing, China, in 2019. He is currently pursuing the Ph.D. degree in electric machine and apparatus with the Harbin University of Science and Technology. His current research interests include permanent magnet vernier motors design and analytical calculation.

LIJING WANG received the B.E. degree in automation from Qiqihar University, Qiqihar, China, in 2012, and the M.S. degree in control science and engineering from the College of Department of Computer and Control Engineering, Qiqihar University, in 2016. She is currently pursuing the Ph.D. degree in electric machine and apparatus with the Harbin University of Science and Technology. Her current research interests include nonlinear control, motor control, pattern recognition, and intelligent systems.